LANGMUIR

pubs.acs.org/Langmuir Article

Comparing Protein Adsorption onto Alumina and Silica Nanomaterial Surfaces: Clues for Vaccine Adjuvant Development

Hyeonjin Park, Gamaliel Junren Ma, Bo Kyeong Yoon, Nam-Joon Cho,* and Joshua A. Jackman*

Cite This: https://dx.doi.org/10.1021/acs.langmuir.0c03396 Read Online

ACCESS | Metrics & More | Article Recommendations

ABSTRACT: Protein adsorption onto nanomaterial surfaces is important for various nanobiotechnology applications such as biosensors and drug delivery. Within this scope, there is growing interest to develop alumina- and silica-based nanomaterial vaccine adjuvants and an outstanding need to compare protein adsorption onto alumina- and silica-based nanomaterial surfaces. Herein, using alumina- and silica-coated arrays of silver nanodisks with plasmonic properties, we conducted localized surface plasmon resonance (LSPR) experiments to evaluate real-time adsorption of bovine serum albumin (BSA) protein onto alumina and silica surfaces. BSA monomers and oligomers were prepared in different water−ethanol mixtures and both adsorbing species consistently showed quicker adsorption kinetics and more extensive adsorption-related spreading on alumina surfaces as compared to on silica surfaces. We rationalized these experimental observations in terms of the electrostatic forces governing protein−surface interactions on the two nanomaterial surfaces and the results support that more rigidly attached BSA protein-based coatings can be formed on alumina-based nanomaterial surfaces. Collectively, the findings in this study provide fundamental insight into protein−surface interactions at nanomaterial interfaces and can help to guide the development of protein-based coatings for medical and biotechnology applications such as vaccines.

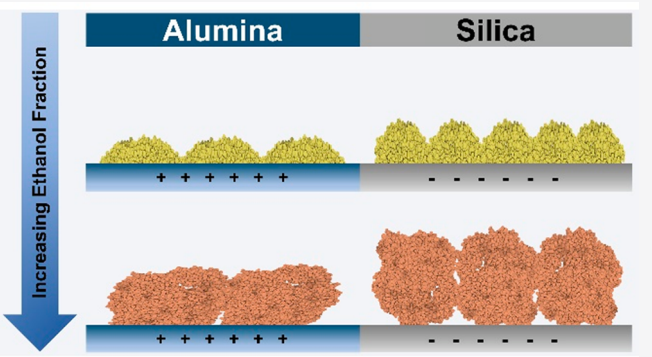

INTRODUCTION

The noncovalent adsorption of protein monomers and oligomers onto inorganic and organic surfaces is widely relevant to various medical and biotechnology applications such as biosensors,[1−3] material biocompatibility,[4,5] and nanomaterial adjuvants.[6−8] There is extensive interest in understanding how various mechanistic factors affect protein adsorption and adsorption-related conformational changes and how controlling such factors can lead to precisely tuned protein-based coatings.[9−13] The fabrication of noncovalently adsorbed, self-assembled protein coatings with user-defined properties falls within the nanoarchitectonics concept[14,15] and the functional presentation of protein molecules such as antigens on nanomaterial surfaces is also important for vaccine adjuvant design.[16,17]

In general, solution-phase proteins have folded secondary structures that impart conformational stability,[18] while there has been growing attention to how modulating solution-phase conformational stability can influence protein adsorption behavior on solid supports. An early example demonstrated that engineered variants of a human enzyme with higher degrees of solution-phase conformational stability exhibited less irreversible binding to solid surfaces and vice versa.[19] Among naturally occurring serum albumin proteins from different animal species, similar trends have been reported, whereby bovine serum albumin (BSA) had lower solution-phase conformational stability and greater irreversible adsorption to solid supports than human and rat analogues.[20] Other experimental studies have further demonstrated that the adsorption behavior of BSA proteins can be influenced by (1) tuning solution-phase conformational properties via environmental conditions and amphipathic stabilizers,[21−24] (2) changing substrate properties such as atomic composition, surface topography, and charge,[25−28] and (3) modulating protein structure, including the extent of denaturation and self-assembled structure (monomer vs oligomer).[29,30] To date, most related protein adsorption studies have been conducted on silica surfaces because silica is one of the most widely used substrates in medical and biotechnology applications, while there remains interest in exploring other types of inorganic surfaces, including nanostructured ones relevant to practical applications.[31,32]

Received: November 26, 2020
Revised: December 22, 2020

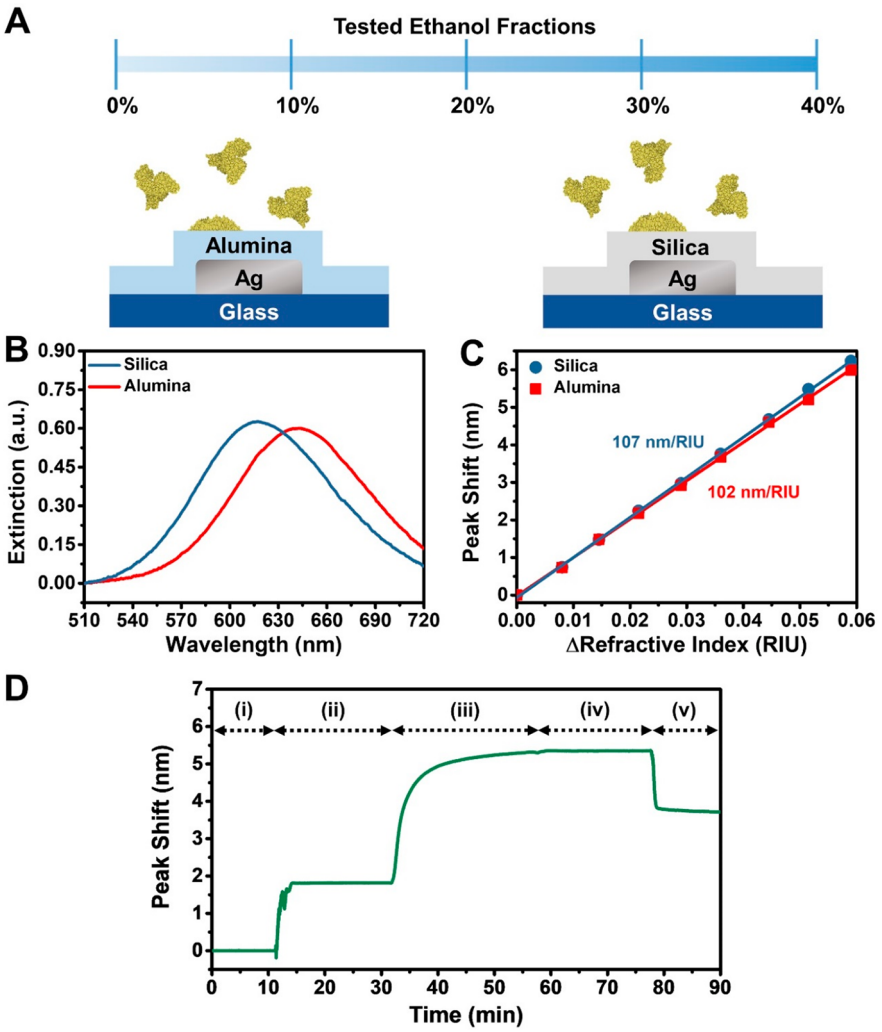

Figure 1. Experimental strategy for tracking protein adsorption onto nanomaterial surfaces. (A) Schematic illustration of the experimental concept to track BSA protein adsorption onto alumina- and silica-coated silver nanodisk arrays in different water−ethanol mixtures. The BSA structure was rendered from Protein Data Bank (PDB) file 3V03. (B) Optical extinction spectra for alumina- and silica-coated silver nanodisk arrays in water. (C) Bulk refractive index sensitivity characterization of alumina- and silica-coated silver nanodisk arrays. The $\Delta\lambda_{max}$ shifts are reported based on titration measurements in water-glycerol mixtures with different refractive index unit (RIU) values. (D) Representative LSPR measurement run for experimental protocol with 100 μM BSA adsorption onto an alumina-coated nanodisk array in 30% ethanol. The stages correspond to (i) baseline signal in water, (ii) solvent exchange to the water−ethanol mixture with 30% ethanol, (iii) BSA protein addition in the equivalent water−ethanol mixture, (iv) washing step with the equivalent water−ethanol mixture (without protein), and (v) washing step with water.

One prominent example is the class of aluminum-based materials such as alumina, which have distinct material properties (e.g., isoelectric point) compared to silica and hence are expected to elicit distinct protein adsorption behaviors. So far, several studies have investigated BSA protein adsorption onto alumina surfaces, however, the main focus has been limited to measuring adsorption uptake as a function of bulk protein concentration.[33−35] There remains an outstanding need to measure real-time BSA adsorption kinetics on alumina surfaces along with the extent of adsorption-related conformational changes and adlayer properties, which can impact the physical stability and functional presentation of adsorbed protein molecules. Moreover, there has been growing interest in utilizing alumina[36,37] and silica[38,39] nanomaterials as immune adjuvants for vaccine development, especially since the adsorption of protein antigens onto the nanomaterial surface can promote antigen stability and enhance antibody production.[40,41]

Herein, we conducted localized surface plasmon resonance (LSPR) experiments to track the real-time adsorption of BSA protein onto alumina- and silica-coated silver nanodisk arrays in different water−ethanol mixtures. By varying the solvent conditions, we were able to prepare BSA monomers and oligomers with different conformational properties and identified that both monomers and oligomers adsorb preferentially onto alumina-coated nanomaterial surfaces with quicker adsorption kinetics indicative of stronger protein−surface interactions. The embedded nanodisk transducers were highly sensitive to protein adsorption-related changes in the local refractive index[42,43] near the alumina and silica surface coatings and the corresponding LSPR measurement readout provided insight into real-time protein adsorption uptake and adsorption-related protein conformational changes on nanomaterial surfaces.[44,45]

https://dx.doi.org/10.1021/acs.langmuir.0c03396
Langmuir XXXX, XXX, XXX−XXX

MATERIALS AND METHODS

Protein Sample Preparation. Fatty acid-free BSA protein (catalog no. A7030) was obtained from Sigma-Aldrich (St. Louis, MO). Lyophilized BSA was solubilized at a mass concentration of 6.6 mg/mL (~100 μM) in the appropriate water−ethanol mixture with 0, 10, 20, 30, or 40% (v/v) ethanol fraction. This protein concentration was selected because it is within the typical range used for surface passivation and coating applications.[25,46,47] The water−ethanol mixtures were prepared using ethanol and deionized water that was obtained from a Milli-Q water purification system (MilliporeSigma, Burlington, MA). The solution pH of the water−ethanol mixtures was maintained around 7.2 ± 0.2 (ref 48). Before experiments, the protein samples were loaded into a syringe and filtered through a poly(ether sulfone) membrane with 200 nm diameter pores (catalog no. 595−4520; Thermo Fisher Scientific, Waltham, MA).

Dynamic Light Scattering (DLS). The size distribution of solution-phase BSA protein molecules in different water−ethanol mixtures at 25 °C was measured by DLS experiments, which were conducted using a 90Plus particle size analyzer (Brookhaven Instruments, Holtsville, NY). The intensity-weighted, Gaussian-fitted distribution of BSA hydrodynamic diameters was determined, as previously described.[2] The mean diameter and standard deviation (SD) of the protein size distribution were reported from n = 5 technical replicates, where SD is defined as the full-width-at-half-maximum (fwhm)/2.355.

Localized Surface Plasmon Resonance (LSPR) Sensing Measurements. An Insplorion XNano instrument (Insplorion AB, Gothenburg, Sweden) was employed to measure BSA protein adsorption onto alumina- and silica-coated silver nanodisk arrays via transmission-mode LSPR measurements, as previously described.[21] The sensor chips were obtained from Insplorion AB and consisted of noninteracting, nonperiodic arrangements of nanodisks, which had been fabricated on top of a transparent glass substrate by hole-mask colloidal lithography.[49] The nanodisk arrays had ~8% surface coverage and the entire substrate surface was then conformally coated with an ~10 nm thick layer of sputtered alumina or silicon nitride. Prior to each experiment, the sensor surfaces were sequentially rinsed with water and ethanol, followed by drying with nitrogen gas and then exposed to oxygen plasma at 50 W radiofrequency power for 1 min using a CUTE-1MPR machine (Femto Science Inc., Hwaseong, Republic of Korea). The latter step removed any residual organic contaminants from both types of sensor surfaces and also resulted in the formation of a silica overlayer on the silicon nitride surface,[50] which was the contacting surface for protein adsorption. After cleaning, the alumina- and silica-coated sensor chips were loaded into a microfluidic chamber for protein adsorption experiments.

In the experiments, the time-resolved optical extinction spectrum of transmitted white light that passed through the sensor surface was measured by UV−vis spectroscopy and collected at a frequency of 1 Hz. The LSPR peak wavelength (λ_{max}) corresponding to the maximum-intensity extinction wavelength in each spectrum was identified based on centroid analysis.[51] The $\Delta\lambda_{max}$ shift due to changes in the local refractive index near the sensor surface was tracked as a function of time. Instrumental operation, data collection, and data analysis were conducted using the Insplorer software package (Insplorion AB). Liquid samples were injected under continuous flow conditions into the microfluidic chamber at a volumetric flow rate of 50 μL/min by using a peristaltic pump.

RESULTS AND DISCUSSION

Experimental Strategy. Biosensing tools have proven useful to characterize the structural and functional properties of protein reagents and pharmaceuticals and motivated our experimental strategy.[52,53] We employed alumina- and silica-coated silver nanodisk arrays with plasmonic properties to comparatively investigate BSA protein adsorption onto the two surfaces (Figure 1A). In addition to fundamental scientific interest in comparing protein adsorption on different surfaces, alumina- and silica-based nanomaterials have also received growing interest as vaccine adjuvants, a role which is related to protein adsorption and adsorption-induced conformational changes. We further studied protein adsorption in different water−ethanol mixtures with 0−40% ethanol fractions because solution-phase BSA undergoes extensive conformational changes across this range of solvent conditions, which can also impact adsorption behavior.[30]

We initially characterized the LSPR extinction properties of the alumina- and silica-coated silver nanodisk arrays in water (Figure 1B). The nanodisk array consisted of ~100 nm diameter and ~20 nm height silver nanodisks that were fabricated on a glass substrate in a random, noninteracting arrangement and the entire substrate was then coated conformally with a ~10 nm-thick alumina- or silica-functionalized overlayer. A maximum-intensity peak wavelength (λ_{max}) was observed in the optical extinction spectrum for each array and the corresponding λ_{max} values were 641 and 617 nm for the alumina- and silica-coated nanodisk arrays, respectively. The experimental results agreed well with theoretical calculations, which predicted λ_{max} values of 627 and 622 nm for alumina- and silica-coated silver nanodisks based on the Drude-Lorentz model and an oblate spheroid approximation.[54,55] The analytical calculations were performed for 100 nm diameter and 20 nm height oblate spheroids with a 10 nm overlayer coating, which is consistent with the as-fabricated nanostructure dimensions. The bulk refractive index sensitivities for both sensor chips were also evaluated by measuring the magnitude of the $\Delta\lambda_{max}$ shift responses upon titration with water-glycerol mixtures that had increasing bulk refractive index values (Figure 1C). The bulk refractive index sensitivities for alumina- and silica-coated nanodisk arrays were determined to be 102 and 107 nm per refractive index unit (RIU), respectively, indicating that both sensing platforms are sensitive to refractometric shifts to similar extents.

We then proceeded to investigate the LSPR measurement responses for 100 μM BSA protein adsorption onto the alumina- and silica-coated sensor surfaces in different water−ethanol mixtures. A representative LSPR measurement run for the 30% ethanol case is shown in Figure 1D and outlines the basic experimental stages, which consisted of (i) a baseline signal in water, followed by (ii) solvent exchange to the appropriate water−ethanol mixture, (iii) BSA protein addition in the equivalent water−ethanol mixture, (iv) washing step with the equivalent water−ethanol mixture (without protein), and (v) washing step with water. Accordingly, three $\Delta\lambda_{max}$ shifts related to the BSA adsorption process were analyzed per experiment as follows: (1) total BSA adsorption uptake in the water−ethanol mixture relative to the water−ethanol mixture without protein (stages ii vs iii); (2) postwash BSA adsorption uptake in the water−ethanol mixture relative to the water−ethanol mixture without protein (stages ii vs iv); and (3) postwash BSA adsorption uptake in water relative to initial water baseline (stages i vs v). As such, the analyzed $\Delta\lambda_{max}$ shifts across the different stages corresponded to changes in local refractive index due to protein adsorption as opposed to changes in the bulk refractive index due to the solution environment. Control experiments were also performed using the same protocol without BSA protein and the three analyzed $\Delta\lambda_{max}$ shifts had negligible magnitudes, which confirmed that the sensing strategy specifically detected the conformational properties of adsorbed protein molecules.

https://dx.doi.org/10.1021/acs.langmuir.0c03396
Langmuir XXXX, XXX, XXX−XXX

DLS Characterization. Prior to LSPR measurements, we first characterized the size distribution of BSA proteins in different water−ethanol mixtures by conducting dynamic light scattering (DLS) experiments. The results support that solution-phase BSA proteins exist as monomers at 0−20% ethanol fractions while they tend to self-assemble into soluble oligomers at 30% and higher ethanol fractions[56] (Table 1).

Table 1. DLS Measurements of BSA Protein Size in Water−Ethanol Mixtures As a Function of Ethanol Fraction[a]

ethanol fraction (%)	BSA hydrodynamic diameter (nm)
0	5.9 ± 2.7
10	5.7 ± 2.7
20	7.4 ± 3.6
30	34.8 ± 18.1
40	99.7 ± 49.7

[a]The data are presented as mean ± standard deviation (SD) from n = 5 measurements.

More specifically, the BSA monomers in water−ethanol mixtures with 0−20% ethanol fractions had hydrodynamic diameters around 5−7 nm, whereas BSA oligomers in water−ethanol mixtures with 30% and 40% ethanol fractions had approximately 35 and 100 nm diameters, respectively. This trend agrees well with past circular dichroism spectroscopy experiments that showed the BSA secondary structure was stable and exhibited a physiologically relevant degree of α-helical character in 0−20% ethanol conditions, while a progressive decrease in BSA α-helicity occurred in 30−40% ethanol conditions.[57] Hence, it was possible to prepare two types of protein colloids in our experiments, BSA monomers and oligomers, and to test their respective adsorption properties.

LSPR Measurements. *BSA Adsorption onto Alumina-Coated Surfaces.* We proceeded to conduct LSPR measurements to track BSA protein adsorption kinetics onto alumina-coated nanodisk arrays in different water−ethanol mixtures. For each water−ethanol mixture series, a measurement baseline was established in the appropriate mixture, and then 100 μM BSA protein in the same mixture was added under continuous flow conditions (Figure 2A, first arrow). A washing step in the same solvent mixture without protein was then performed after BSA adsorption saturation was reached (Figure 2A, second arrow).

There was rapid adsorption uptake in all cases while the specific $\Delta\lambda_{max}$ shift response depended on the solvent condition. In 0% ethanol (pure water), the $\Delta\lambda_{max}$ shift for BSA protein adsorption at saturation was around 2.11 nm (Figure 2A, pink circles). Similar levels of protein adsorption were observed in 10% and 20% ethanol, with $\Delta\lambda_{max}$ shifts around 2.33 and 2.35 nm, respectively (Figure 2A, blue up-triangles and green down-triangles). On the other hand, larger $\Delta\lambda_{max}$ shifts of 3.15 and 3.32 nm were observed in 30 and 40% ethanol, respectively (Figure 2A, orange diamonds and purple squares). The transition in $\Delta\lambda_{max}$ shift magnitudes appears to be related to the adsorbing species since BSA monomers adsorb in ≤20% ethanol conditions while BSA oligomers adsorb in ≥30% ethanol conditions.

In addition to the ethanol-dependent trend observed with BSA adsorption at saturation, distinct changes in the adsorbate properties occurred upon a solvent washing step with the equivalent water−ethanol mixtures. For direct comparison, the

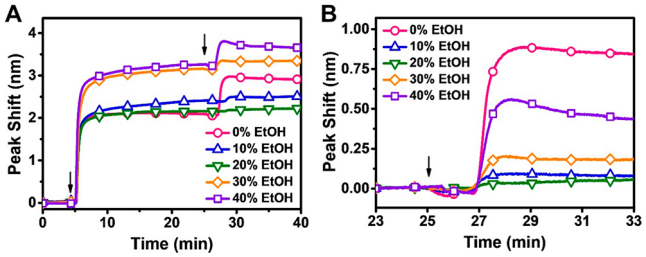

Figure 2. Real-time adsorption kinetics of BSA protein on alumina-coated plasmonic nanodisk arrays. (A) Time-resolved LSPR $\Delta\lambda_{max}$ shift responses for 100 μM BSA protein adsorption onto alumina-coated sensor surfaces in different water−ethanol mixtures. The ethanol fraction in the water−ethanol mixtures is denoted by % EtOH. The initial condition corresponds to the sensor surface in the appropriate water−ethanol mixture, followed by addition of 100 μM BSA protein in the equivalent water−ethanol mixture at around t = 5 min (see arrow 1) and then solvent washing with the equivalent water−ethanol mixture at around t = 25 min (see arrow 2). (B) Magnified view of the normalized LSPR $\Delta\lambda_{max}$ shift responses for the solvent washing step corresponding to the data in panel (A).

$\Delta\lambda_{max}$ shift responses for the solvent washing step are presented in Figure 2B, in which case the baseline signals correspond to the BSA protein adlayers at saturation before washing. While solvent washing for BSA protein adlayers in high-salt aqueous conditions typically results in some protein desorption,[9] we observed that the BSA proteins were rigidly attached in all tested cases and exhibited densification upon washing, as indicated by positive $\Delta\lambda_{max}$ shifts in the measurement responses.[30] In 0% ethanol, there was a positive $\Delta\lambda_{max}$ shift value of around 0.82 nm due to solvent washing, which indicates densification of the protein adlayer as opposed to protein desorption. By contrast, appreciably smaller $\Delta\lambda_{max}$ shift values of around 0.15 nm or less occurred upon solvent washing in the 10% and 20% ethanol cases. A modestly larger $\Delta\lambda_{max}$ shift of around 0.23 nm occurred in 30% ethanol, while a much larger $\Delta\lambda_{max}$ shift of around 0.45 nm occurred in 40% ethanol. These data support that both BSA monomers and oligomers adsorbed irreversibly on the alumina surface and can undergo structural rearrangements upon washing the adsorbate.

BSA Adsorption onto Silica-Coated Surfaces. Similar LSPR measurements were performed to track BSA protein adsorption kinetics onto silica-coated nanodisk arrays in different water−ethanol mixtures. For each water−ethanol mixture series, a measurement baseline was established in the appropriate mixture, and then 100 μM BSA protein in the same mixture was added under continuous flow conditions (Figure 3A, first arrow). A washing step in the same solvent mixture without protein was then performed after BSA adsorption saturation (Figure 3A, second arrow).

In 0−20% ethanol, BSA adsorption yielded similar $\Delta\lambda_{max}$ shifts of around 3.05, 2.88, and 3.03 nm, respectively (Figure 3A, pink circles, blue up-triangles, and green down-triangles). By contrast, BSA adsorption in 30% and 40% ethanol yielded larger $\Delta\lambda_{max}$ shifts of around 3.51 and 3.54 nm, respectively (Figure 3A, orange diamonds and purple squares). The transition in $\Delta\lambda_{max}$ shift magnitudes for protein adsorption onto silica surfaces mirrors the trend observed on alumina surfaces and supports that the adsorption of BSA monomers and oligomers yielded distinct measurement responses.

https://dx.doi.org/10.1021/acs.langmuir.0c03396
Langmuir XXXX, XXX, XXX−XXX

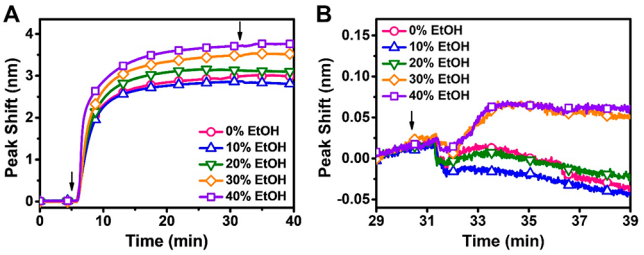

Figure 3. Real-time adsorption kinetics of BSA protein on silica-coated plasmonic nanodisk arrays. (A) Time-resolved LSPR $\Delta\lambda_{max}$ shift responses for 100 μM BSA protein adsorption onto silica-coated sensor surfaces in different water−ethanol mixtures. The ethanol fraction in the water−ethanol mixtures is denoted by % EtOH. The initial condition corresponds to the sensor surface in the appropriate water−ethanol mixture, followed by addition of 100 μM BSA protein in the equivalent water−ethanol mixture at around t = 5 min (see arrow 1) and then solvent washing with the equivalent water−ethanol mixture at around t = 30 min (see arrow 2). (B) Magnified view of the normalized LSPR $\Delta\lambda_{max}$ shift responses for the solvent washing step corresponding to the data in panel (A).

A magnified view of the normalized $\Delta\lambda_{max}$ shift responses for the solvent washing step is also presented in Figure 3B. In 0−20% ethanol, there were nearly negligible $\Delta\lambda_{max}$ shifts of less than 0.05 nm due to solvent washing while modestly larger $\Delta\lambda_{max}$ shifts of around 0.07 nm occurred in 30−40% ethanol. Hence, both BSA monomers and oligomers adsorbed stably to the sensor surface and the overall trend in adsorption behavior at saturation is also consistent with our past results on silica-coated gold nanodisk arrays.[30]

Comparison of Protein Adsorption Uptake. To compare the measurement data obtained with the two sensor surfaces, we normalized the $\Delta\lambda_{max}$ shifts according to the corresponding bulk refractive index sensitivities so that the data are presented in universal refractive index units (RIU) (Figure 4). The normalized data for BSA adsorption uptake at saturation are presented in Figure 4A. In 0−20% ethanol, there were larger peak shifts of around 0.025 RIU due to BSA adsorption on silica while the corresponding peak shifts were around 0.02 RIU on alumina. In 30−40% ethanol, the peak shifts were around 0.03 RIU on both surfaces. These results support that the adsorption of BSA oligomers yields larger measurement responses than those of BSA monomers. Furthermore, the adsorption-related unfolding of BSA monomers appears to be more sensitive to the substrate properties of the sensor surface while adsorption of BSA oligomers involves larger adsorbing species with more complex rearrangement processes in the adsorbed state. In the latter case of oligomers, only the constituent monomers that come into contact with the sensor surface undergo adsorption-related unfolding.[20,29]

More specifically, BSA protein adsorption on alumina led to smaller measurement responses than on silica. This effect was most pronounced for monomer adsorption and is likely related to stronger protein−surface interactions on alumina surfaces by virtue of attractive electrostatic interactions. Indeed, alumina has an isoelectric point around pH 8.7 (ref 58) and is hence positively charged under the test conditions while BSA is negatively charged with an isoelectric point around pH 5.4 (ref 59). On the other hand, silica has an isoelectric point around pH 3.9 (ref 58) and is also negatively charged, which results in more repulsive electrostatic interactions with adsorbing BSA protein molecules. As such, adsorbed BSA molecules on alumina surfaces undergo greater adsorption-related unfolding and spreading due to stronger protein−surface interactions, which results in fewer adsorbed BSA molecules per surface area and consequently a smaller measurement response. Of note, BSA oligomer adsorption gave rise to more similar measurement responses on the two sensor surfaces because, unlike free BSA monomers, BSA oligomers were unable to fully undergo extensive adsorption-related deformation of all constituent monomers within the oligomeric species and hence were less affected by the distinct protein−surface interactions on each surface.

In addition, the normalized data for BSA adsorption after washing with the appropriate water−ethanol mixture are presented in Figure 4B. A similar trend in RIU values to that of the adsorption saturation data described above was found for adsorbed BSA after solvent washing on the two surfaces, supporting that the adsorbed monomers and oligomers remained attached on both surfaces. Notably, one key difference was that the solvent washing steps for adsorbed BSA on alumina surfaces caused more appreciable peak shift increases at all tested ethanol fractions while positive peak shift increases were only observed for BSA adlayers on silica in 30−40% ethanol fractions and were smaller in magnitude.

After solvent washing, an additional washing step was conducted using deionized water and the corresponding normalized data for BSA adsorption after this second washing step are presented in Figure 4C. In this case, the reported data

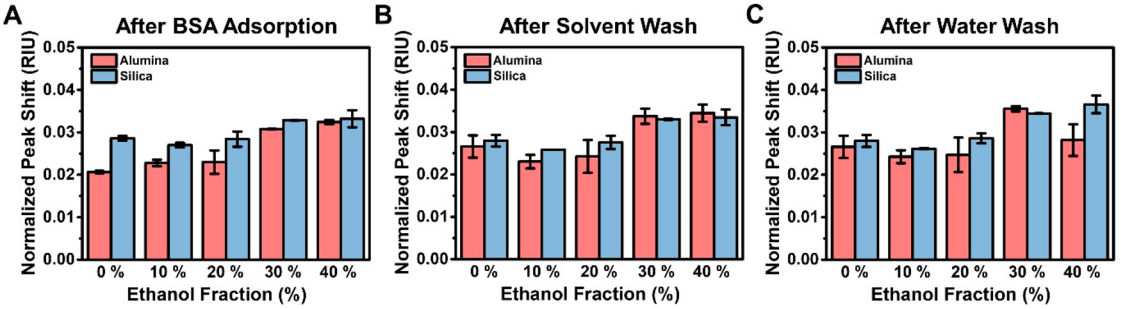

Figure 4. Comparison of LSPR measurement responses for BSA protein adsorption onto alumina and silica surfaces. (A) Normalized LSPR ΔRIU shift responses for BSA adsorption saturation in different water−ethanol mixtures (relative to the water−ethanol mixture baseline without protein). (B) Normalized LSPR ΔRIU shift responses for BSA adsorption upon washing in different water−ethanol mixtures (relative to the water−ethanol mixture baseline without protein). (C) Normalized LSPR ΔRIU shift responses for BSA adsorption upon washing in water (relative to the water baseline without protein). The data are presented as mean ± standard deviation (SD) from n = 3 measurements.

https://dx.doi.org/10.1021/acs.langmuir.0c03396
Langmuir XXXX, XXX, XXX−XXX

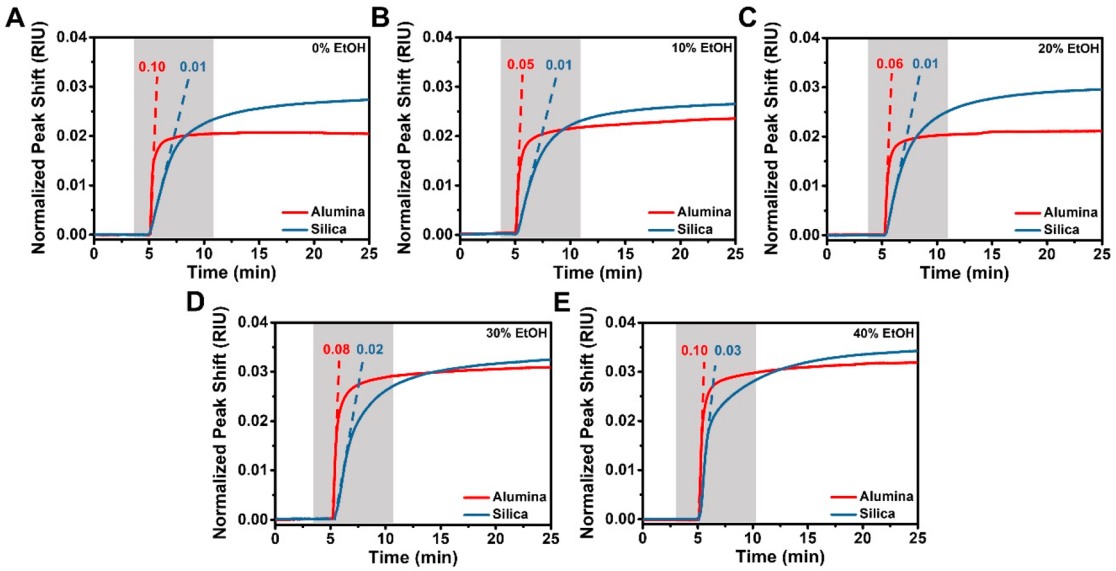

Figure 5. Comparison of BSA protein adsorption kinetics on alumina and silica surfaces. (A–E) Time-resolved LSPR ΔRIU shifts are presented for BSA adsorption in different water–ethanol mixtures. The initial rates of change in the LSPR signal were determined by linear fits and the mean values are reported in RIU/min units from n = 3 measurements.

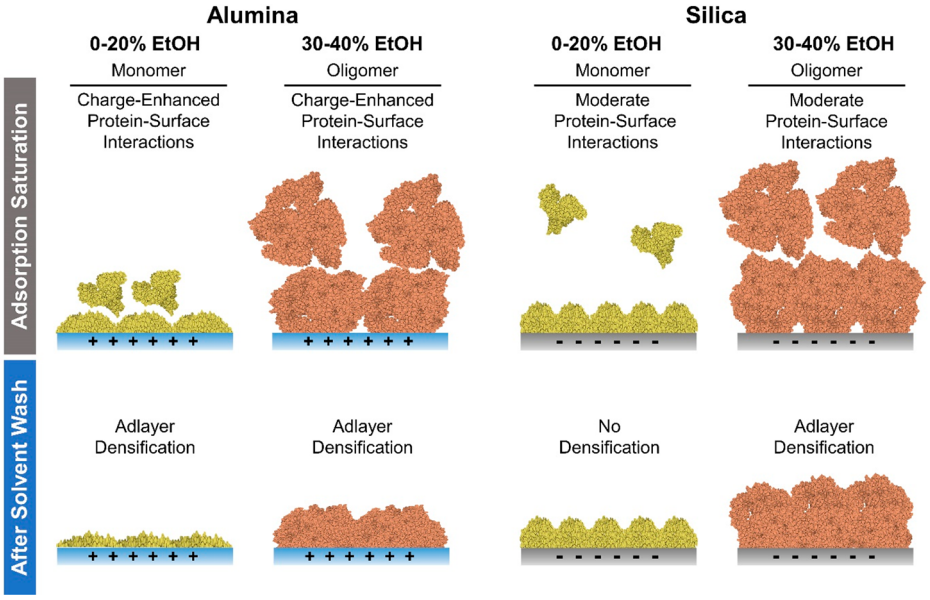

Figure 6. Schematic illustration comparing the adsorption behavior of BSA proteins on alumina and silica surfaces. In general, BSA monomers and oligomers underwent greater adsorption-induced deformation on the positively charged alumina surface compared to on the negatively charged silica surface due to charge-enhanced protein–surface interactions.

were normalized to the initial water baseline and a similar trend in RIU values was observed on the two surfaces, further supporting that the BSA adlayers remained largely stable on the sensor surfaces. One noteworthy aspect is that we used deionized water for the final washing step in this study, whereas a high-salt buffer solution was used during the final washing step in a previous study which caused extensive desorption of adsorbed BSA molecules on silica surfaces.[30] This distinction between the use of different aqueous solutions for the washing step reinforces the importance of electrostatic forces in modulating adsorbed protein stability and this approach can help to fabricate more well-packed protein adlayers, especially in combination with subsequent cross-linking strategies.[23]

Comparison of BSA Protein Adsorption Kinetics. In addition to protein adsorption uptake, the corresponding adsorption kinetics in different water–ethanol mixtures were compared across the two surfaces, as presented in Figure 5. Under equivalent solution conditions, BSA adsorption tended to reach adsorption saturation more quickly on alumina surfaces than on silica surfaces. Quantitatively, we further analyzed the adsorption kinetics by calculating the initial slope of the normalized LSPR measurement responses. Since protein adsorption is a diffusion-limited process,[60] the rate of contacting protein molecules depends on the flow conditions and protein specifics (e.g., hydrodynamics). As such, the rate of contacting protein molecules was equivalent for the protein adsorption experiments on both nanomaterial surfaces because

https://dx.doi.org/10.1021/acs.langmuir.0c03396
Langmuir XXXX, XXX, XXX–XXX

the relevant experimental conditions were standardized. On the other hand, the rate of change in the LSPR measurement response is influenced by the net adsorption and desorption of attached BSA molecules on the sensor surface and varies according to the nanomaterial surface properties. More specifically, the extent of protein desorption process depends inversely on the strength of protein−surface interactions whereby a larger rate of change in the LSPR signal indicates comparatively less desorption and vice versa.

For 0−20% ethanol fractions, the average initial slopes for BSA adsorption onto the alumina and silica surfaces were ∼0.07 and ∼0.01 RIU/min, respectively (Figures 5A−C). Moreover, for 30−40% ethanol fractions, the average initial slopes for BSA adsorption onto the alumina and silica surfaces were ∼0.09 and ∼0.03 RIU/min, respectively (Figures 5D,E). The larger slope values for BSA adsorption onto the alumina surface across all tested solvent conditions support that there are stronger protein−surface interactions on alumina due to attractive electrostatic interactions, which result in an appreciably lower desorption rate compared to that on the silica surface. Indeed, it was previously shown that >99% of attached BSA protein molecules rapidly desorb from silica surfaces due to a low sticking coefficient and short adsorption lifetime.[61]

Interestingly, larger initial slope values were also observed with BSA oligomers in 30−40% ethanol as opposed to BSA monomers in 0−20% ethanol, especially on the silica surface. Since the diffusion-limited adsorption rate for BSA monomers is much greater than for BSA oligomers, these results support that BSA oligomers have much stronger interactions with the surface, likely due to more pinning sites.[29] This effect is most pronounced on the silica surface, in which case the protein−surface interactions are relatively weaker overall, while the effect is still prominent on the alumina surface as well.

Trends in BSA Adsorption Behavior. Figure 6 presents a set of schematic illustrations comparing the adsorption behavior of BSA proteins on alumina and silica surfaces. The scenarios are divided into cases involving the adsorption of BSA monomers and oligomers in water−ethanol mixtures with low (0−20%) and high (30−40%) ethanol fractions, respectively.

On positively charged alumina surfaces, negatively charged BSA monomers and oligomers underwent more extensive adsorption-related unfolding and spreading, which resulted in relatively low total adsorption uptake due to a greater adsorption footprint per attached monomer or oligomer. Furthermore, upon solvent washing, protein adlayer densification was observed across all tested ethanol fractions on the alumina surface, as indicated by increases in the LSPR measurement response. This densification arose from the wash-induced desorption of BSA monomers or oligomers that were weakly adsorbed on the initially formed adlayer, which in turn enabled greater spreading of the remaining adlayer molecules due to less steric confinement. More specifically, it is likely that BSA proteins initially adsorbed onto the alumina surface in a manner whereby protein regions with positive surface charge character were oriented away from the sensor surface due to electrostatic repulsion.[33] Such conformational restrictions tend to inhibit the degree of spreading and Rezwan et al. have also discussed how BSA proteins could still adsorb onto a preformed BSA monolayer on an alumina surface through protein−protein interactions.[34] Upon solvent washing, weakly adsorbed protein molecules are removed from the surface, which decreases steric hindrance within the adsorbate and enables remaining, firmly attached protein molecules to spread out to a greater extent, resulting in closer proximity of adsorbed BSA molecules, on average, to the sensor surface that yielded larger measurement responses.

On the other hand, on negatively charged silica surfaces, adsorbing BSA proteins had relatively weaker protein−surface interactions. At low ethanol fractions, there was irreversible protein adsorption but no densification upon solvent washing. At higher ethanol fractions, a modest degree of densification was observed but to a lower extent than on alumina. Modest densification of BSA adlayers on silica upon solvent washing has been attributed to a combination of ethanol-induced protein unfolding and lower conformational flexibility. Overall, these findings demonstrate that BSA monomers and oligomers have stronger interactions with alumina surfaces than with silica surfaces, as indicated by quicker adsorption kinetics and more rigidly attached adlayer coatings.

CONCLUSIONS

In this study, we utilized the LSPR sensing technique to investigate the real-time adsorption of BSA monomers and oligomers onto alumina- and silica-coated silver nanodisk arrays in different water−ethanol mixtures. Across the range of tested conditions, it was observed that both protein species, BSA monomers and oligomers, had stronger protein−surface interactions on alumina surfaces, as indicated by quicker adsorption kinetics to reach saturation and more rigid adlayer packing. In general, these findings are consistent with electrostatic forces playing an important role in modulating protein attachment since BSA had a net negative charge while alumina and silica had net positive and negative charges, respectively.

In addition to alumina, other classes of aluminum-based materials such as aluminum hydroxide have also been widely utilized as nanomaterial vaccine adjuvants.[62] While alumina has an isoelectric point around pH 8.7 (ref 58), the isoelectric point of aluminum hydroxide is even higher at around pH 11 (ref 63) and, hence, aluminum hydroxide would also be positively charged under our test conditions. Accordingly, a similar trend in BSA adsorption behavior might be anticipated on aluminum hydroxide as on alumina, and there has also been past interest in comparing the adjuvant effects of aluminum hydroxide and silica nanomaterials.[64] While BSA is a model protein, there are a wide range of other antigens with different conformational and surface charge properties that can be used together with nanomaterial adjuvants and the measurement approach in this study is broadly applicable to study the adsorption properties of protein antigens on various classes of nanomaterial surfaces as well.

AUTHOR INFORMATION

Corresponding Authors

Nam-Joon Cho − *School of Materials Science and Engineering, Nanyang Technological University, 639798, Singapore;* orcid.org/0000-0002-8692-8955; Email: njcho@ntu.edu.sg

Joshua A. Jackman − *School of Chemical Engineering, Sungkyunkwan University, Suwon 16419, Republic of Korea;* orcid.org/0000-0002-1800-8102; Email: jjackman@skku.edu

https://dx.doi.org/10.1021/acs.langmuir.0c03396
Langmuir XXXX, XXX, XXX−XXX

Authors

Hyeonjin Park − *School of Chemical Engineering, Sungkyunkwan University, Suwon 16419, Republic of Korea; School of Materials Science and Engineering, Nanyang Technological University, 639798, Singapore*

Gamaliel Junren Ma − *School of Materials Science and Engineering, Nanyang Technological University, 639798, Singapore;* orcid.org/0000-0002-6740-1031

Bo Kyeong Yoon − *School of Chemical Engineering, Sungkyunkwan University, Suwon 16419, Republic of Korea*

Complete contact information is available at: https://pubs.acs.org/10.1021/acs.langmuir.0c03396

Notes

The authors declare no competing financial interest.

■ ACKNOWLEDGMENTS

We acknowledge support from the Samsung Research Fund, Sungkyunkwan University, 2019. Graphical illustrations were created with BioRender.com under an academic lab subscription.

■ REFERENCES

(1) del Río, J. S.; Henry, O. Y.; Jolly, P.; Ingber, D. E. An antifouling coating that enables affinity-based electrochemical biosensing in complex biological fluids. *Nat. Nanotechnol.* **2019**, *14* (12), 1143−1149.

(2) Ma, G. J.; Ferhan, A. R.; Jackman, J. A.; Cho, N.-J. Conformational flexibility of fatty acid-free bovine serum albumin proteins enables superior antifouling coatings. *Commun. Mater.* **2020**, *1* (1), 45.

(3) Bhakta, S. A.; Evans, E.; Benavidez, T. E.; Garcia, C. D. Protein adsorption onto nanomaterials for the development of biosensors and analytical devices: A review. *Anal. Chim. Acta* **2015**, *872*, 7−25.

(4) Firkowska-Boden, I.; Zhang, X.; Jandt, K. D. Controlling protein adsorption through nanostructured polymeric surfaces. *Adv. Healthcare Mater.* **2018**, *7* (1), 1700995.

(5) Zeuthen, C. M.; Shahrokhtash, A.; Fromell, K.; Ekdahl, K. N.; Mohammad-Beigi, H.; Sutherland, D. S. C1q recognizes antigen-bound IgG in a curvature-dependent manner. *Nano Res.* **2020**, *13*, 1651−1658.

(6) Pinholt, C.; Hartvig, R. A.; Medlicott, N. J.; Jorgensen, L. The importance of interfaces in protein drug delivery−why is protein adsorption of interest in pharmaceutical formulations? *Expert Opin. Drug Delivery* **2011**, *8* (7), 949−964.

(7) Reed, S. G.; Orr, M. T.; Fox, C. B. Key roles of adjuvants in modern vaccines. *Nat. Med.* **2013**, *19* (12), 1597−1608.

(8) HogenEsch, H.; O'Hagan, D. T.; Fox, C. B. Optimizing the utilization of aluminum adjuvants in vaccines: you might just get what you want. *npj Vaccines* **2018**, *3* (1), 1−11.

(9) Rabe, M.; Verdes, D.; Seeger, S. Understanding protein adsorption phenomena at solid surfaces. *Adv. Colloid Interface Sci.* **2011**, *162* (1−2), 87−106.

(10) Tsapikouni, T. S.; Missirlis, Y. F. Protein−material interactions: From micro-to-nano scale. *Mater. Sci. Eng., B* **2008**, *152* (1−3), 2−7.

(11) Lahari, C.; Jasti, L. S.; Fadnavis, N. W.; Sontakke, K.; Ingavle, G.; Deokar, S.; Ponrathnam, S. Adsorption induced enzyme denaturation: the role of polymer hydrophobicity in adsorption and denaturation of α-chymotrypsin on allyl glycidyl ether (AGE)-ethylene glycol dimethacrylate (EGDM) copolymers. *Langmuir* **2010**, *26* (2), 1096−1106.

(12) Pan, H.; Qin, M.; Meng, W.; Cao, Y.; Wang, W. How do proteins unfold upon adsorption on nanoparticle surfaces? *Langmuir* **2012**, *28* (35), 12779−12787.

(13) Marruecos, D. F.; Schwartz, D. K.; Kaar, J. L. Impact of surface interactions on protein conformation. *Curr. Opin. Colloid Interface Sci.* **2018**, *38*, 45−55.

(14) Ariga, K.; Nishikawa, M.; Mori, T.; Takeya, J.; Shrestha, L. K.; Hill, J. P. Self-assembly as a key player for materials nanoarchitectonics. *Sci. Technol. Adv. Mater.* **2019**, *20* (1), 51−95.

(15) Ariga, K.; Li, J.; Fei, J.; Ji, Q.; Hill, J. P. Nanoarchitectonics for dynamic functional materials from atomic-/molecular-level manipulation to macroscopic action. *Adv. Mater.* **2016**, *28* (6), 1251−1286.

(16) Zhou, X.; Jiang, X.; Qu, M.; Aninwene, G. E.; Jucaud, V.; Moon, J. J.; Gu, Z.; Sun, W.; Khademhosseini, A. Engineering antiviral vaccines. *ACS Nano* **2020**, *14* (10), 12370−12389.

(17) Jackman, J. A.; Yoon, B. K.; Ouyang, L.; Wang, N.; Ferhan, A. R.; Kim, J.; Majima, T.; Cho, N.-J. Biomimetic nanomaterial strategies for virus targeting: Antiviral therapies and vaccines. *Adv. Funct. Mater.* **2020**, 2008352.

(18) Dobson, C. M.; Šali, A.; Karplus, M. Protein folding: a perspective from theory and experiment. *Angew. Chem., Int. Ed.* **1998**, *37* (7), 868−893.

(19) Karlsson, M.; Ekeroth, J.; Elwing, H.; Carlsson, U. Reduction of irreversible protein adsorption on solid surfaces by protein engineering for increased stability. *J. Biol. Chem.* **2005**, *280* (27), 25558−25564.

(20) Ma, G. J.; Ferhan, A. R.; Sut, T. N.; Jackman, J. A.; Cho, N.-J. Understanding how natural sequence variation in serum albumin proteins affects conformational stability and protein adsorption. *Colloids Surf., B* **2020**, *194*, 111194.

(21) Jackman, J. A.; Ferhan, A. R.; Yoon, B. K.; Park, J. H.; Zhdanov, V. P.; Cho, N.-J. Indirect nanoplasmonic sensing platform for monitoring temperature-dependent protein adsorption. *Anal. Chem.* **2017**, *89* (23), 12976−12983.

(22) Givens, B. E.; Diklich, N. D.; Fiegel, J.; Grassian, V. H. Adsorption of bovine serum albumin on silicon dioxide nanoparticles: Impact of pH on nanoparticle−protein interactions. *Biointerphases* **2017**, *12* (2), 02D404.

(23) Park, J. H.; Sut, T. N.; Jackman, J. A.; Ferhan, A. R.; Yoon, B. K.; Cho, N.-J. Controlling adsorption and passivation properties of bovine serum albumin on silica surfaces by ionic strength modulation and cross-linking. *Phys. Chem. Chem. Phys.* **2017**, *19* (13), 8854−8865.

(24) Ma, G. J.; Ferhan, A. R.; Jackman, J. A.; Cho, N.-J. Elucidating how different amphipathic stabilizers affect BSA protein conformational properties and adsorption behavior. *Langmuir* **2020**, *36* (35), 10606−10614.

(25) Jeyachandran, Y.; Mielczarski, E.; Rai, B.; Mielczarski, J. Quantitative and qualitative evaluation of adsorption/desorption of bovine serum albumin on hydrophilic and hydrophobic surfaces. *Langmuir* **2009**, *25* (19), 11614−11620.

(26) Zeng, H.; Chittur, K. K.; Lacefield, W. R. Analysis of bovine serum albumin adsorption on calcium phosphate and titanium surfaces. *Biomaterials* **1999**, *20* (4), 377−384.

(27) Givens, B. E.; Xu, Z.; Fiegel, J.; Grassian, V. H. Bovine serum albumin adsorption on SiO_2 and TiO_2 nanoparticle surfaces at circumneutral and acidic pH: A tale of two nano-bio surface interactions. *J. Colloid Interface Sci.* **2017**, *493*, 334−341.

(28) Rezwan, K.; Studart, A. R.; Vörös, J.; Gauckler, L. J. Change of ζ potential of biocompatible colloidal oxide particles upon adsorption of bovine serum albumin and lysozyme. *J. Phys. Chem. B* **2005**, *109* (30), 14469−14474.

(29) Park, J. H.; Jackman, J. A.; Ferhan, A. R.; Ma, G. J.; Yoon, B. K.; Cho, N.-J. Temperature-induced denaturation of BSA protein molecules for improved surface passivation coatings. *ACS Appl. Mater. Interfaces* **2018**, *10* (38), 32047−32057.

(30) Tan, J. Y. B.; Yoon, B. K.; Ma, G. J.; Sut, T. N.; Cho, N.-J.; Jackman, J. A. Unraveling how ethanol-induced conformational changes affect BSA protein adsorption onto silica surfaces. *Langmuir* **2020**, *36* (31), 9215−9224.

(31) Nugroho, F. A. A.; Frost, R.; Antosiewicz, T. J.; Fritzsche, J.; Larsson Langhammer, E. M.; Langhammer, C. Topographically flat

nanoplasmonic sensor chips for biosensing and materials science. *ACS Sensors* **2017**, *2* (1), 119−127.
(32) Ferhan, A. R.; Yoon, B. K.; Jeon, W.-Y.; Jackman, J. A.; Cho, N.-J. Unraveling how nanoscale curvature drives formation of lysozyme protein monolayers on inorganic oxide surfaces. *Appl. Mater. Today* **2020**, *20*, 100729.
(33) Urano, H.; Fukuzaki, S. Conformation of adsorbed bovine serum albumin governing its desorption behavior at alumina-water interfaces. *J. Biosci. Bioeng.* **2000**, *90* (1), 105−111.
(34) Rezwan, K.; Meier, L. P.; Rezwan, M.; Vörös, J.; Textor, M.; Gauckler, L. J. Bovine serum albumin adsorption onto colloidal Al_2O_3 particles: a new model based on zeta potential and UV−Vis measurements. *Langmuir* **2004**, *20* (23), 10055−10061.
(35) Gispert, M.; Serro, A.; Colaço, R.; Saramago, B. Bovine serum albumin adsorption onto 316L stainless steel and alumina: a comparative study using depletion, protein radiolabeling, quartz crystal microbalance and atomic force microscopy. *Surf. Interface Anal.* **2008**, *40* (12), 1529−1537.
(36) Maquieira, Á.; Brun, E. M.; Garces-Garcia, M.; Puchades, R. Aluminum oxide nanoparticles as carriers and adjuvants for eliciting antibodies from non-immunogenic haptens. *Anal. Chem.* **2012**, *84* (21), 9340−9348.
(37) Bilyy, R.; Paryzhak, S.; Turcheniuk, K.; Dumych, T.; Barras, A.; Boukherroub, R.; Wang, F.; Yushin, G.; Szunerits, S. Aluminum oxide nanowires as safe and effective adjuvants for next-generation vaccines. *Mater. Today* **2019**, *22*, 58−66.
(38) Carvalho, L. V.; Ruiz, R. d. C.; Scaramuzzi, K.; Marengo, E. B.; Matos, J. R.; Tambourgi, D. V.; Fantini, M. C.; Sant'Anna, O. A. Immunological parameters related to the adjuvant effect of the ordered mesoporous silica SBA-15. *Vaccine* **2010**, *28* (50), 7829−7836.
(39) Mahony, D.; Cavallaro, A. S.; Stahr, F.; Mahony, T. J.; Qiao, S. Z.; Mitter, N. Mesoporous silica nanoparticles act as a self-adjuvant for ovalbumin model antigen in mice. *Small* **2013**, *9* (18), 3138−3146.
(40) Mannhalter, J.; Neychev, H.; Zlabinger, G.; Ahmad, R.; Eibl, M. Modulation of the human immune response by the non-toxic and non-pyrogenic adjuvant aluminium hydroxide: effect on antigen uptake and antigen presentation. *Clin. Exp. Immunol.* **1985**, *61* (1), 143−151.
(41) Colaprico, A.; Senesi, S.; Ferlicca, F.; Brunelli, B.; Ugozzoli, M.; Pallaoro, M.; O'Hagan, D. T. Adsorption onto aluminum hydroxide adjuvant protects antigens from degradation. *Vaccine* **2020**, *38* (19), 3600−3609.
(42) Larsson, E. M.; Edvardsson, M. E.; Langhammer, C.; Zorić, I.; Kasemo, B. A combined nanoplasmonic and electrodeless quartz crystal microbalance setup. *Rev. Sci. Instrum.* **2009**, *80* (12), 125105.
(43) Jackman, J. A.; Ferhan, A. R.; Cho, N.-J. Surface-based nanoplasmonic sensors for biointerfacial science applications. *Bull. Chem. Soc. Jpn.* **2019**, *92* (8), 1404−1412.
(44) Jackman, J. A.; Ferhan, A. R.; Cho, N.-J. Nanoplasmonic sensors for biointerfacial science. *Chem. Soc. Rev.* **2017**, *46* (12), 3615−3660.
(45) Oh, S.-H.; Altug, H. Performance metrics and enabling technologies for nanoplasmonic biosensors. *Nat. Commun.* **2018**, *9*, 5263.
(46) Jeyachandran, Y.; Mielczarski, J.; Mielczarski, E.; Rai, B. Efficiency of blocking of non-specific interaction of different proteins by BSA adsorbed on hydrophobic and hydrophilic surfaces. *J. Colloid Interface Sci.* **2010**, *341* (1), 136−142.
(47) Mahmood, T.; Yang, P.-C. Western blot: technique, theory, and trouble shooting. *N. Am. J. Med. Sci.* **2012**, *4* (9), 429.
(48) Kotrba, M.; Schilling, L.-H. In *Measurement of pH in Ethanol, Distilled Water, and their Mixtures: On the Assessment of pH in Ethanol-Based Natural History Wet Collections and the Detrimental Aspects of Dilution with Distilled Water*; Collection Forum, Soc. for the Pres. of Natural History Collections, 2017; pp 84−101.
(49) Fredriksson, H.; Alaverdyan, Y.; Dmitriev, A.; Langhammer, C.; Sutherland, D. S.; Zäch, M.; Kasemo, B. Hole−mask colloidal lithography. *Adv. Mater.* **2007**, *19* (23), 4297−4302.
(50) Kennedy, G.; Buiu, O.; Taylor, S. Oxidation of silicon nitride films in an oxygen plasma. *J. Appl. Phys.* **1999**, *85* (6), 3319−3326.
(51) Dahlin, A. B.; Tegenfeldt, J. O.; Höök, F. Improving the instrumental resolution of sensors based on localized surface plasmon resonance. *Anal. Chem.* **2006**, *78* (13), 4416−4423.
(52) Bracke, N.; Barhdadi, S.; Wynendaele, E.; Gevaert, B.; D'Hondt, M.; De Spiegeleer, B. Surface acoustic wave biosensor as a functional quality method in pharmaceutics. *Sens. Actuators, B* **2015**, *210*, 103−112.
(53) Yao, H.; Fernández, C. S.; Xu, X.; Wynendaele, E.; De Spiegeleer, B. A Surface Acoustic Wave (SAW) biosensor method for functional quantification of E. coli l-asparaginase. *Talanta* **2019**, *203*, 9−15.
(54) Langhammer, C.; Schwind, M.; Kasemo, B.; Zoric, I. Localized surface plasmon resonances in aluminum nanodisks. *Nano Lett.* **2008**, *8* (5), 1461−1471.
(55) Langhammer, C.; Yuan, Z.; Zorić, I.; Kasemo, B. Plasmonic properties of supported Pt and Pd nanostructures. *Nano Lett.* **2006**, *6* (4), 833−838.
(56) Yoshizawa, S.; Arakawa, T.; Shiraki, K. Dependence of ethanol effects on protein charges. *Int. J. Biol. Macromol.* **2014**, *68*, 169−172.
(57) Yoshikawa, H.; Hirano, A.; Arakawa, T.; Shiraki, K. Effects of alcohol on the solubility and structure of native and disulfide-modified bovine serum albumin. *Int. J. Biol. Macromol.* **2012**, *50* (5), 1286−1291.
(58) Cuddy, M. F.; Poda, A. R.; Brantley, L. N. Determination of isoelectric points and the role of pH for common quartz crystal microbalance sensors. *ACS Appl. Mater. Interfaces* **2013**, *5* (9), 3514−3518.
(59) Shi, Q.; Zhou, Y.; Sun, Y. Influence of pH and ionic strength on the steric mass-action model parameters around the isoelectric point of protein. *Biotechnol. Prog.* **2005**, *21* (2), 516−523.
(60) Zhdanov, V.; Kasemo, B. Monte Carlo simulation of the kinetics of protein adsorption. *Proteins: Struct., Funct., Genet.* **1998**, *30* (2), 177−182.
(61) Kwok, K.; Yeung, K.; Cheung, N. Adsorption kinetics of bovine serum albumin on fused silica: population heterogeneities revealed by single-molecule fluorescence microscopy. *Langmuir* **2007**, *23* (4), 1948−1952.
(62) Moyer, T. J.; Kato, Y.; Abraham, W.; Chang, J. Y. H.; Kulp, D. W.; Watson, N.; Turner, H. L.; Menis, S.; Abbott, R. K.; Bhiman, J. N.; Melo, M. B.; Simon, H. A.; Herrera-De la Mata, S.; Liang, S.; Seumois, G.; Agarwal, Y.; Li, N.; Burton, D. R.; Ward, A. B.; Schief, W. R.; Crotty, S.; Irvine, D. J. Engineered immunogen binding to alum adjuvant enhances humoral immunity. *Nat. Med.* **2020**, *26* (3), 430−440.
(63) Rinella, J. V.; White, J. L.; Hem, S. L. Treatment of aluminium hydroxide adjuvant to optimize the adsorption of basic proteins. *Vaccine* **1996**, *14* (4), 298−300.
(64) Mancino, D.; Ovary, Z. Adjuvant effects of amorphous silica and of aluminium hydroxide on IgE and IgG1 antibody production in different inbred mouse strains. *Int. Arch. Allergy Immunol.* **2004**, *61* (3), 253−258.

https://dx.doi.org/10.1021/acs.langmuir.0c03396
Langmuir XXXX, XXX, XXX−XXX